European Journal of Medicinal Chemistry 74 (2014) 73–84

Contents lists available at ScienceDirect

European Journal of Medicinal Chemistry

journal homepage: http://www.elsevier.com/locate/ejmech

Original article

Design, synthesis, biological evaluation, and comparative docking study of 1,2,4-triazolones as CB1 receptor selective antagonists

Shuang Han [a], Fei-Fei Zhang [b], Xin Xie [b], Jian-Zhong Chen [a,*]

[a] College of Pharmaceutical Sciences, Zhejiang University, Hangzhou, Zhejiang 310058, China
[b] CAS Key Laboratory of Receptor Research, National Center for Drug Screening, Shanghai Institute of Materia Medica, Chinese Academy of Sciences, China

ARTICLE INFO

Article history:
Received 6 July 2013
Received in revised form
21 November 2013
Accepted 19 December 2013
Available online 31 December 2013

Keywords:
Cannabinoid receptors
Antagonist
1,2,4-Triazolone
Scaffold hopping
Homology model

ABSTRACT

Cannabinoids are potentially useful for the treatment of several diseases. In the present work, we report the syntheses and biological evaluations of 1,2,4-triazolone derivatives designed using a combined approach of scaffold hopping and pharmacophore-oriented method. These compounds exhibited interesting antagonistic activity to the cannabinoid CB1 receptor. The preliminary structure–activity relationships were further discussed. In addition, docking simulations were performed on the good bioactive compound **5c** and the low potent compound **5d**, respectively, on the basis of homology models of the CB1 and CB2 receptors, which were constructed based on human β2-adrenoreceptor and optimized in a membrane environment by MD simulations. Calculation of the binding modes gave us insights into the structural requirements for improving the cannabinoid receptor bioactivity and selectivity.

1. Introduction

Cannabinoid (CB) receptors belong to the rhodopsin-like G protein-coupled receptors (GPCRs) family. Up to now, it has been identified of two subtypes of cannabinoid receptors, namely, CB1 receptor and CB2 receptor [1]. The CB1 receptor is predominantly located within the central nervous system (CNS) and also identified in peripheral nerve terminals and other cell types, while the CB2 receptor is expressed mainly in the peripheral immune tissues and cells. Activation of either CB1 or CB2 receptor mediates inhibition of adenylate cyclase and activation of mitogen-activated protein (MAP) kinase [2,3]. In addition, the CB1 receptor's activation also results in inhibition of N- and P/Q-type calcium channels and stimulation of potassium channels. The endocannabinoid system (ECS) comprises the cannabinoid receptors, endocannabinoids, and the corresponding enzymes involved in synthesis and degradation of endocannabinoids. The pharmacological studies have shown that the ECS regulates many physiological functions and processes including pain, energy balance, emotional regulation, etc [4–7]. For instance, S-777469 [8] (structure A in Fig. 1), as a CB2 receptor agonist, has completed phase II clinical trials for the treatment of atopic dermatitis. Yang et al. [9–11] reported the novel trisubstituted sulfonamides and bisamide derivatives as the CB2 receptor inverse agonists showing potent inhibitory activity on RANKL-induced osteoclast formation, which offered a wonderful beginning to develop a novel agent for the treatment of osteoporosis. The CB1 receptor selective antagonists were effective as therapeutic agents for obesity and related chronic diseases, such as type II diabetes, cardiovascular disease [12,13]. For example, Rimonabant (SR141716A, structure B in Fig. 1) was developed as an anti-obesity drug by reducing food intake in Europe. However, Rimonabant was withdrawn from the market owing to its significant psychiatric side effects. By now, the treatment choices of obesity are limited while the number of obesity people is increasing in every year, so there remains a significantly unsatisfied need for the development of anti-obesity agents. Rimonabant displays comprehensive pharmacological effects for obesity and associated metabolic disorders, indicating the CB1 receptor is an attractive target for drug discovery [14]. In order to avoid the adverse effects in CNS, the new strategy is designing novel ligands of the CB1 receptor with lower blood–brain barrier (BBB) penetration [15].

In recent years, the identification and optimization of novel cannabinoid ligand has been a hot topic in drug discovery [16]. The first reported CB1 receptor selective antagonist, SR141716A ([N-(piperidin-1-yl)-5-(4-chlorophenyl)-1-(2,4-dichlorophenyl)-4-methyl-1H-pyrazole-3-carboxamide]), was discovered by Sanofi-Aventis in 1994 [17]. Later, SR144528 ([N-[(1S)-*endo*-1,3,3-trimethylbicycle[2.2.1]-heptan-2-yl]-5-(4-chloro-3-methylphenyl

* Corresponding author. Tel.: +86 571 88208659.
E-mail address: chjz@zju.edu.cn (J.-Z. Chen).

0223-5234/$ – see front matter © 2013 Elsevier Masson SAS. All rights reserved.
http://dx.doi.org/10.1016/j.ejmech.2013.12.018

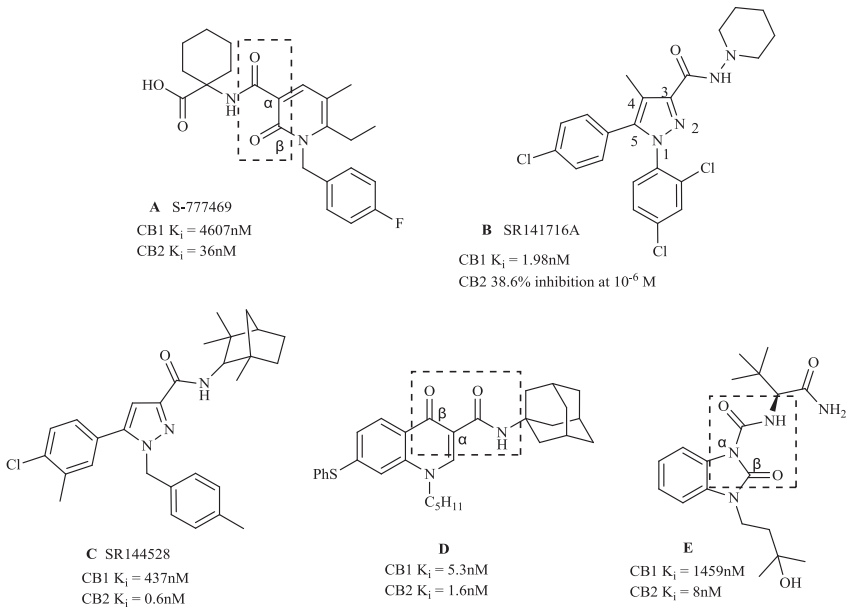

Fig. 1. Chemical structures of some known cannabinoid ligands.

)-1-(4-methylbenzyl)-pyrazole-3-carboxamide], structure **C** in Fig. 1), an analog of SR141716A, was developed to be the first CB2 receptor selective inverse agonist/antagonist [18,19]. With further research of the potent diarylpyrazole derivatives, several structural modifications were achieved on the basis of these parent compounds. Some compounds with different substituents on the pyrazole ring or the carboxamide part were synthesized [20–24], and others were prepared with isosteric replacement of the pyrazole core structure [25–27]. In the meantime, a number of cannabinoid ligands with different chemical scaffolds have emerged. As shown in Fig. 1, bioactive cannabinoid compounds **A**, **D** [28], and **E** [29] share similarly structural characteristics containing a carbonyl group at the β-position of the carboxamide part, inducing a privileged structure for designing original cannabinoid ligands. In addition, the scaffold hopping strategy is a useful approach for drug discovery by modifying the core structure of promising compounds. Combination of scaffold hopping and bioisostere method has been previously applied in identification of novel cannabinoid ligands [30,31].

In the present paper, we describe the design, syntheses, biological evaluations, preliminary structure–activity relationship (SAR) analyses, and docking simulations of a new serious of cannabinoid ligands with 1,2,4-triazolone scaffold. At first, the structural skeleton was designed using a combined method of scaffold hopping and privileged structure-oriented approaches. Structural modifications were then carried out with guideline of a pharmacophore model derived from the previous reported 3D-QSAR model [32]. The cell-based calcium current assays were applied to study the functional activity of synthesized 1,2,4-triazolone derivatives. The bioactive tests indicated that our designed compounds displayed interesting antagonistic activity towards either CB1 or CB2 receptor.

In order to calculate the interaction modes of our synthesized 1,2,4-triazolones binding to the CB1 and CB2 receptors, respectively, 3D homology models of both CB1 and CB2 receptors were constructed based on the crystal structure of β2-adrenergic receptor [33], and the conformations of both CB receptors were then optimized by molecular dynamics (MD) simulations with the proteins embedded in a hydrate bilayer system. Based on the generated homology models of both CB1 and CB2 receptors, flexible docking simulations were performed to gain insight to the receptor-ligand interactions and to explain the possibly selective characteristics of the compounds with different substituents. The docking simulations provided more information on the differences between the two binding sites of CB1 and CB2 receptors, which would afford guidelines for the design of new cannabinoid ligand with improved bioactive and selective profiles.

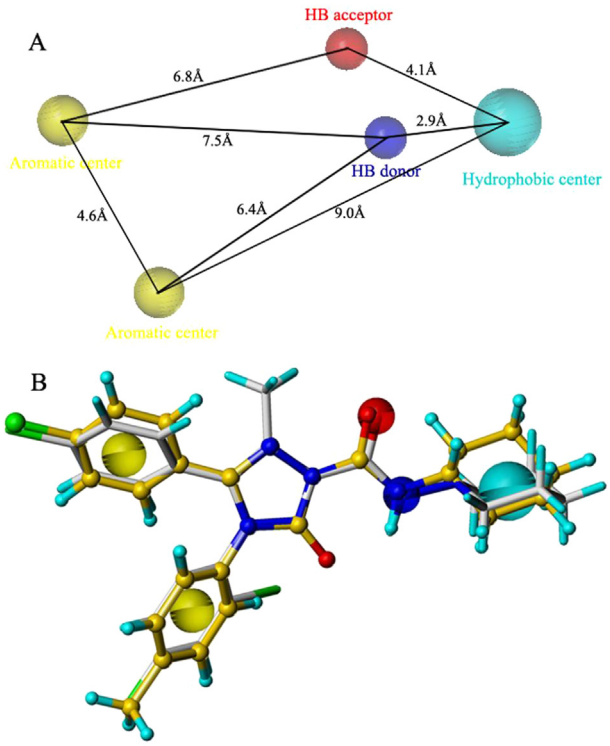

Fig. 2. Pharmacophore model based on the reported favorable conformation of pyrazole compounds for the CB1 receptor (A) and molecular alignment of both SR141716A, which carbon atoms were drawn in white, and typical compound of 1,2,4-triazolone with carbon atoms colored in orange (B). (For interpretation of the references to color in this figure legend, the reader is referred to the web version of this article.)

Table 1
Chemical structures and *in vitro* cannabinoid receptor activity of 1,2,4-triazolones (**5a**–**m**).

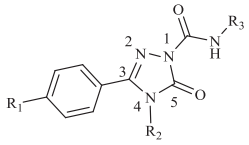

No.	R_1	R_2	R_3	CB1 inhibition/%[a]	CB1 IC_{50}/nM[b]	CB2 inhibition/%[a]	CB2 IC_{50}/nM[b]
5a	Cl	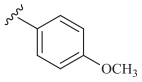		98.6	388	94.0	1510
5b	Cl	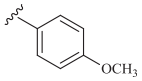	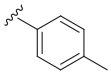	74.6	8440	85.6	20000
5c	Cl	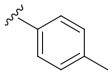		102.2	222	46.4	NT
5d	Cl	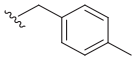		42.6	NT	87.7	1930
5e	Cl	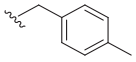	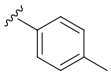	36.8	NT	−55.3	NT
5f	OCH_3	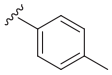		98.0	1840	130.8	4090
5g	OCH_3	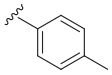	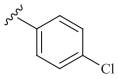	90.5	4730	43.6	NT
5h	CH_3	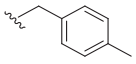		60.9	17800	132.3	5030
5i	CH_3	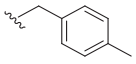	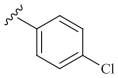	89.0	3750	29.9	NT
5j	CH_3	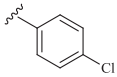		98.2	2100	58.5	NT
5k	CH_3	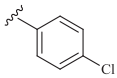	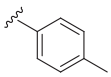	91.9	947	−25.7	NT
5l	OCH_3	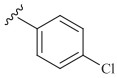	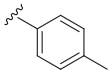	96.6	2280	74.0	NT
5m	OCH_3	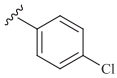		96.5	878	123.5	6080
JTE-907				37.6	NT	129.5	644
SR141716A				100.0	13	100.0	9800

[a] CB1 and CB2 receptors inhibition (% basal) at 10 μM ligand concentration.
[b] NT = not tested.

2. Results and discussion

2.1. Compound design

Chen et al. [32] carried out a combined study by computational 3D-QSAR CoMFA and 2D NMR method on pyrazole compounds to explore the structural requirements for both CB1 and CB2 receptors, and the results provided us helpful criteria for the development of novel bioactive cannabinoid ligands. As illustrated in Fig. 2A, we first extracted the pharmacophore model of ligand for the CB1 receptor according to the preferred conformation of AM263 embedded in 3D-QSAR model [32]. 1,2,4-triazolone ring was applied to replace the pyrazole ring according to the discipline of scaffold hopping strategy. The substitutions were then designed on the basis of 3D-QSAR models generated with the pyrazole derivatives [32]. As illustrated in the reported CoMFA contour maps, a

para-substituted phenyl group was good for bioactivity at 5-position of the pyrazole ring (Fig. 1). In addition, the red area of the CB1 3D-QSAR model in this region suggested a negatively partial-charged unit would increase ligand's bioactivity, while a yellow contour in the corresponding part of the CB2 3D-QSAR model indicated the steric bulky groups would not be favored for the CB2 receptor. Therefore, as the general structure given in Table 1, it was designed to introduce the groups of chlorine, methyl, and methoxyl, respectively, to study the influence of subunits with different electric charge at R_1 part of our designed 1,2,4-triazolone compounds. The CB1 3D-QSAR model had a red region around the 4-position on pyrazole, while by contrast, blue and yellow contours were displayed in the reported CB2 3D-QSAR model, which implied an increasing negatively partial-charged group was superior for CB1 affinity. Herein, a third nitrogen atom was introduced at the corresponding 2-position of 1,2,4-triazolone ring with the purpose of further improving CB1 selectivity. Both CoMFA models showed red contours near the carbonyl oxygen and blue contours near the amide nitrogen, indicating this part was favored for both CB1 and CB2 receptors, so the amide moiety was maintained to be H-bond donor and acceptor, respectively, for the newly designed compounds. Moreover, large yellow areas were displayed around the N-substituted amide in both 3D-QSAR models, implying limited binding pockets were presented in both CB receptors. Therefore, we selected cyclohexyl and substituted phenyl subunits based on the favorable groups of lead pyrazoles. CoMFA models gave contrasting steric maps around the 1-position group of pyrazole, which suggested this group could play a key role in affecting the selectivity for the subtypes of CB receptors, and an aromatic ring was favored for CB1 receptor affinity. Consequently, we introduced substituted phenyl and benzyl groups to study their influence on bioactivity for both receptors. As shown in Fig. 2B, a typical compound was selected from the designed 1,2,4-triazolones to be aligned with SR141716A based on the pharmacophore model, and their conformations were consistent with each other.

2.2. Chemistry

The general procedure for the syntheses of 1,2,4-triazolone derivatives was summarized in Scheme 1. Our successful syntheses of 1,2,4-triazolones were started with *para*-position substituted benzoic acids **1**. The esters **2** were formed by refluxing the acids in MeOH with sulfuric acid as a catalyst, and then the esters were converted to the acid hydrazides **3** by refluxing with an excess of hydrazine hydrate [34]. Reactions of hydrazides **3** and isocyanates gave aroylsemicarbazides, and cyclization of these semicarbazides in refluxing aqueous sodium hydroxide afforded compounds **4** [35,36]. Reactions of the intermediates **4** with different isocyanates produced the 1,2,4-triazolones **5a**–**m**.

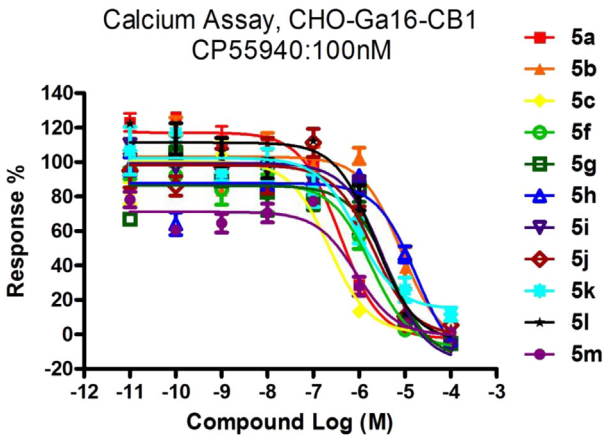

Fig. 3. Whole-cell calcium assays using CHO cells expressing human CB1 receptor and Gα15/16. All experiments were performed in triplicate.

2.3. Biological evaluations and SAR analyses

Fluorescent imaging plate reader technology [37] has played a significant role in high-throughput screening (HTS) for GPCR and ion channel targets [38–40]. The above synthesized 1,2,4-triazolone derivatives, as well as the positive controls SR141716A and JTE-907 [41] were evaluated with their functional activity for the CB1 and CB2 receptors, respectively, on the cell-based calcium current assays. Table 1 summarizes their structures and the corresponding CB1 and CB2 receptors inhibitory activity. In addition, Fig. 3 illustrates all ligands' IC_{50} curves obtained from the assays for the CB1 receptor. The results indicated that most of the newly synthesized compounds presented the CB1 receptor antagonistic activity with IC_{50} values ranging from 222 nM to 17.8 μM, and some compounds had the IC_{50} values in the range of 1.51 μM–20 μM to the CB2 receptor.

The differences at R_2 and R_3 regions of the compounds influenced their bioactivity for the subtypes of cannabinoid receptors. The substituted phenyl group at R_2 part was demonstrated a superior CB1 receptor inhibitory activity over the CB2 receptor (**5a**–**c**, **5f**–**g**, **5j**–**5m**). Remarkably, a substituted benzyl group introduced on R_2 position resulted in an obvious increase in ligand's bioactivity and selectivity for the CB2 receptor (**5d**, **5h**). For R_3 group, either substituted phenyl or cyclohexyl group was tolerated for the CB1

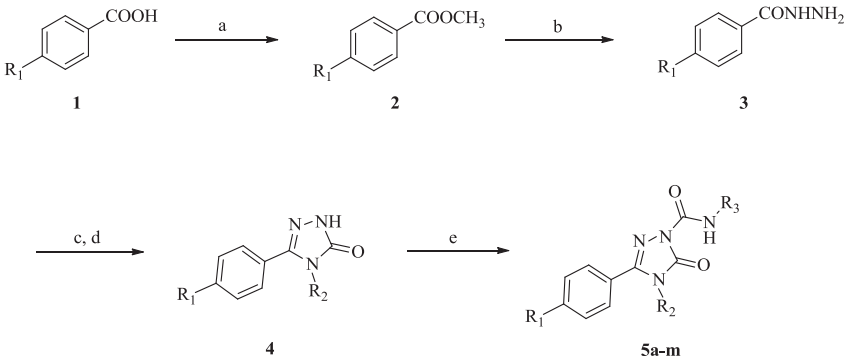

Scheme 1. Reagents and conditions: (a) *conc.* H_2SO_4, MeOH, reflux, 24 h; (b) excess NH_2NH_2, EtOH, reflux, 5 h; (c) R_2NCO, THF, reflux, 24 h; (d) 1 N NaOH(aq), reflux, 24 h; (e) R_3NCO, DBU, CH_3CN, reflux, overnight.

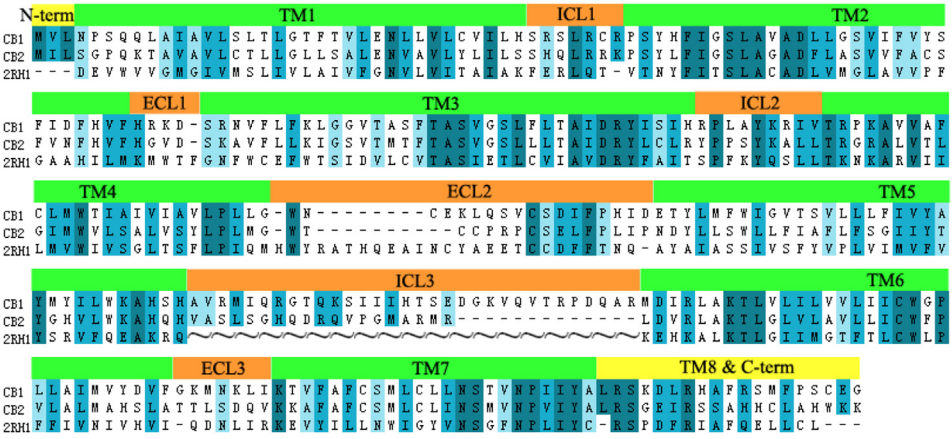

Fig. 4. Sequence alignment of CB1, CB2, and β2-adrenergic receptors. Conserved residues are displayed with blue background, and the T4L part of 2RH1 is not shown in this figure for short. (For interpretation of the references to color in this figure legend, the reader is referred to the web version of this article.)

receptor bioactivity, and the cyclohexyl group was generally helpful (**5a** > **5b**, **5f** > **5g**, **5m** > **5l**). On the other hand, comparing compounds **5d** *vs.* **5e**, and **5h** *vs.* **5i**, the substituted phenyl group at R_3 led to abolish the CB2 receptor bioactivity. Various substituents for the R_1 part showed similar bioactivity. Usually, a chlorine atom was more favored than methyl or methoxyl (**5c** > **5f**, **5d** > **5h**) group. The *in vitro* active data are congruent with the published CoMFA results [32], as discussed in the section of Compound design, of the parent pyrazole compounds.

2.4. Generations of homology models

The 1,2,4-triazolone derivatives displayed interesting antagonistic activity to the CB1 and CB2 receptors, which attracted our attention for further exploring the binding modes of these compounds with the cannabinoid receptors. Since both CB1 and CB2 receptors are membrane proteins, their crystal structures still remain experimentally unresolved. In the past years, many 3D models of the cannabinoid receptors have been generated based on the Rhodopsin's crystal structure [42–45]. Recent breakthroughs in crystallographic studies of GPCRs, as well as the homology modeling method, would help us to build more accurate homology models of cannabinoid receptors. Recently, some successful CB1 and CB2 receptor models [46–51] were also reported based on the X-ray structure of β2-adrenergic receptor (β2-AR) [33], which shares higher identity with the CB receptors than Rhodopsin. However, these generated homology models were not put into a membrane environment for MD optimizations. In order to simulate the interaction modes of our synthesized compounds binding to the CB1 and CB2 receptors, we built up our own coordinates for the structural models of both CB1 and CB2 receptors based on the crystal structure of β2-AR [33] with a general procedure of homology modeling and MD refinements in a membrane environment.

At first, we constructed the homology models of both CB1 and CB2 receptors to represent their active state based on the X-ray structure of β2-adrenergic receptor [33] with high resolution. Both CB1 and CB2 receptors enclose most of the highly conserved residues and motifs in GPCRs superfamily, such as D(E)RY in the third transmembrane domain (TM3), CWXP in TM6, and NPXXY in TM7, which is helpful for sequence alignment and homology model generation. Fig. 4 shows the sequence alignment results of CB1, CB2, and β2 (PDB code: 2RH1) receptors. On the grounds that all the GPCRs have conserved secondary structure in the transmembrane regions, seven TM helixes and one juxtamembrane helix of the CB1 or CB2 receptor were produced directly based on the coordinates of corresponding domains of β2-AR. The structures of loop regions connected the TM domains were obtained using loop search from the whole PDB bank. It was selected manually of the conformations of loops according to the most reasonable alignment and the smallest root mean square deviation value (RMSD) at the terminal residues of the structurally conserved regions (SCR). In addition, based on the references reported before [42,52], both CB1 and CB2 receptors contain a disulfide bridge in second extracellular loop. In the present models, the S–S bonds which formed between Cys257 and Cys264 in the CB1 receptor as well as Cys174 and Cys179 in the CB2 receptor were also taken into account.

2.5. MD simulations

The conformations from homology modeling were refined by MD simulations using AMBER 11 software package [53]. Considering that both CB receptors are membrane proteins, the initially generated homology structures were respectively embedded into a pre-equilibrated aqueous membrane system [54]. The MD simulations were then performed for each of the whole protein/DPPC/TIP3P systems. In order to keep the active conformations of our ligand-free receptors, in the equilibration process the force

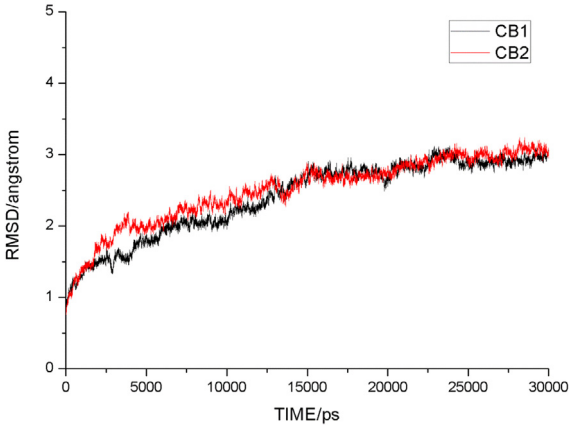

Fig. 5. Backbone RMSD for both apo CB1 receptor (black) and ligand-free CB2 receptor (red) trajectories of production simulation. (For interpretation of the references to color in this figure legend, the reader is referred to the web version of this article.)

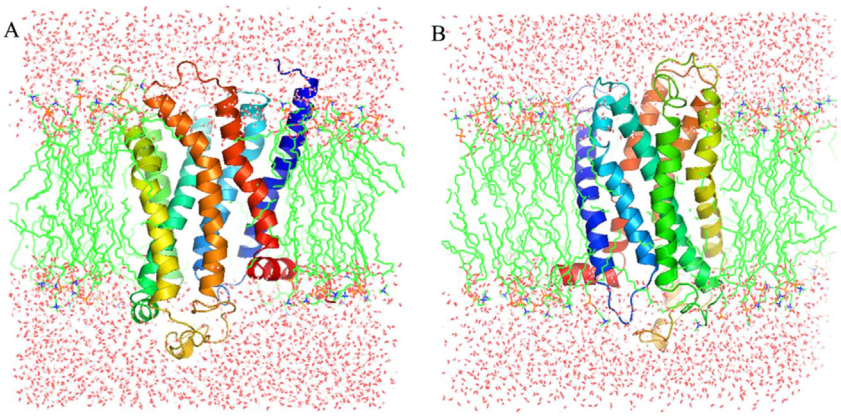

Fig. 6. MD refined conformations of CB1/DPPC/TIP3P complex (A) and CB2/DPPC/TIP3P system (B). The proteins display in cartoon mode, and carbon atoms of DPPC are colored in green. (For interpretation of the references to color in this figure legend, the reader is referred to the web version of this article.)

restraint weight on the atoms of backbone was slowly decreased from 50 to 1 kcal/(mol Å) step by step. During the 30 ns production simulations, the backbone atoms of the helical domains were still restrained with a small force constant of 1 kcal/(mol Å), while the loop regions and the side chains of all the residues were free for minimization. As shown in Fig. 5, the RMSD of the backbone atoms were calculated for each system. The conformations of both proteins kept stable during the last 15 ns of production. After 30 ns MD simulations, the refined conformations of both receptors were extracted for further docking study. Fig. 6 shows the final conformations of both CB receptors in the DPPC/TIP3P system. As indicated in Fig. 7 for the Ramachandran $\psi-\Phi$ distribution plots of the CB receptors, 96.1% of the residues located in the favored regions and other 3.9% resided in allowed areas for the model of the CB1 receptor, while for the CB2 receptor model, the number was 94.6% and 5.4%, respectively. Subsequently, the accuracy and validity of each model was tested with the profiles-3D [55] program of Accelrys Discovery Studio 2.5.5 [56]. The MD-optimized homology models of the CB1 and CB2 receptors were scored 145.3 and 148.7, respectively, comparing with the corresponding expected high value of 140.6 and 133.8 and lowest possible score of 63.3 and 60.2. The results of profiles-3D analysis indicated both generated CB1 and CB2 models would be rationalities with high probabilities.

2.6. Analyses of interaction modes

Since the 1,2,4-triazolone derivatives exhibited weaker bioactivity than the lead compound SR141716A under the conditions of our bioassays, we first investigated the differences between the binding modes of SR141716A and compound **5c**, respectively, with the generated homology model of the CB1 receptor by flexible docking studies using Sybyl-X1.3/FlexiDock [57]. Fig. 8A shows the docking simulated interaction mode between SR141716A and the CB1 receptor, which correlates with its binding conformation calculated by Salo et al. [43]. The critical lysine K192 [43] and the amide oxygen atom of SR141716A forms a hydrogen bond with the length and angle of 2.54 Å and 170.2°, respectively. Furthermore, McAllister et al. [58] reported the binding of SR141716A was affected by the F200A, W279A and W356A mutations, indicating these residues are part of the binding site. In our simulated model, the *p*-Cl phenyl moiety contacts with a hydrophobic cavity composed by the residues V196, F200, W356, and L360 of the CB1 receptor. The 2,4-dichlorophenyl group situates in another hydrophobic cleft formed by W279 and M363, and it is observed a parallel $\pi-\pi$ stacking consisting of three aromatic rings from 2,4-dichlorophenyl, W279, and Y275. The importance of aromatic stacking at Y275 for ligand recognition has been demonstrated by

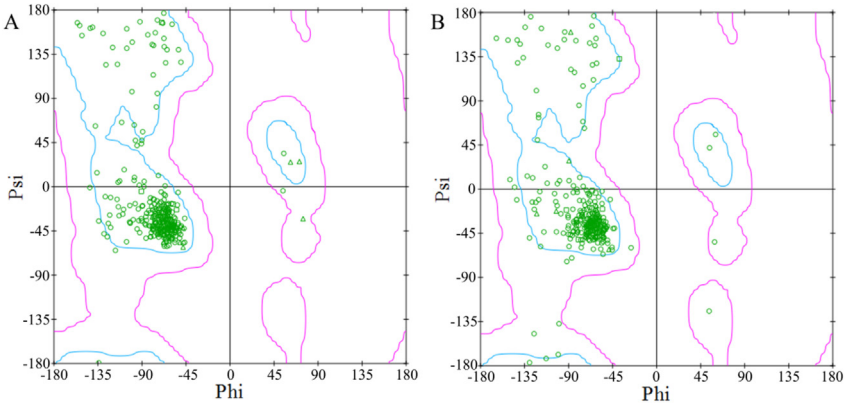

Fig. 7. Ramachandran plot for the MD refined CB1 receptor (A) and CB2 receptor (B) homology model. Glycine residues are displayed as triangles, prolines are shown as squares, and other residues are illustrated as circles. The regions surrounded by blue lines are the favorable areas, and sections enclosed by purple lines are the allowed areas. (For interpretation of the references to color in this figure legend, the reader is referred to the web version of this article.)

McAllister et al. [59] through site mutation and modeling studies. In addition, the piperidyl group inserts into the third pocket surrounded by F177, F189, and W255. Later on, the docking-simulated CB1-**5c** complex was superimposed on the CB1-SR141716A model based on the backbone atoms of the CB1 receptor as shown in Fig. 8A. It is indicated compound **5c** shares quite similar binding mode with SR141716A in the same active site of the CB1 receptor. Moreover, it is accepted that the aromatic and hydrophobic interactions are crucial for affinity of cannabinoid ligands [60,61].

On the other hand, the C4 methyl group on the pyrazole ring forms hydrophobic interaction with the side chain of residue V196 in the docking-simulated CB1-SR141716A complex (Fig. 8A). However, such a hydrophobic interaction is missing in the binding mode of compound **5c** with the CB1 receptor since introducing the third nitrogen atom at the corresponding position of its core ring. In addition, SR141716A contains a much more hydrophobic 2,4-dichlorophenyl moiety in the corresponding region, which can produce stronger π−π interaction to boost CB1 receptor activity, by comparing with the 4-methylphenyl group at R_2 position of compound **5c**. These results probably explain that compound **5c** has lower CB1 receptor bioactivity than SR141716A. Combined with the bioactive data obtained from calcium current assays, the docking simulations further imply that it could be beneficial for improving the CB1 receptor bioactivity by increasing the lipophilicity of substituents on the core scaffold. The results would provide a helpful guideline for future structural optimization on our synthesized compounds.

Consequently, among the 1,2,4-triazolone derivatives we synthesized, compounds **5c** and **5d**, which only had a slight difference at R_2 part, displayed the contrast selectivity for the subtype of cannabinoid receptors. Compound **5c** with a *p*-tolyl group exhibited the best inhibitory activity and selectivity for the CB1 receptor

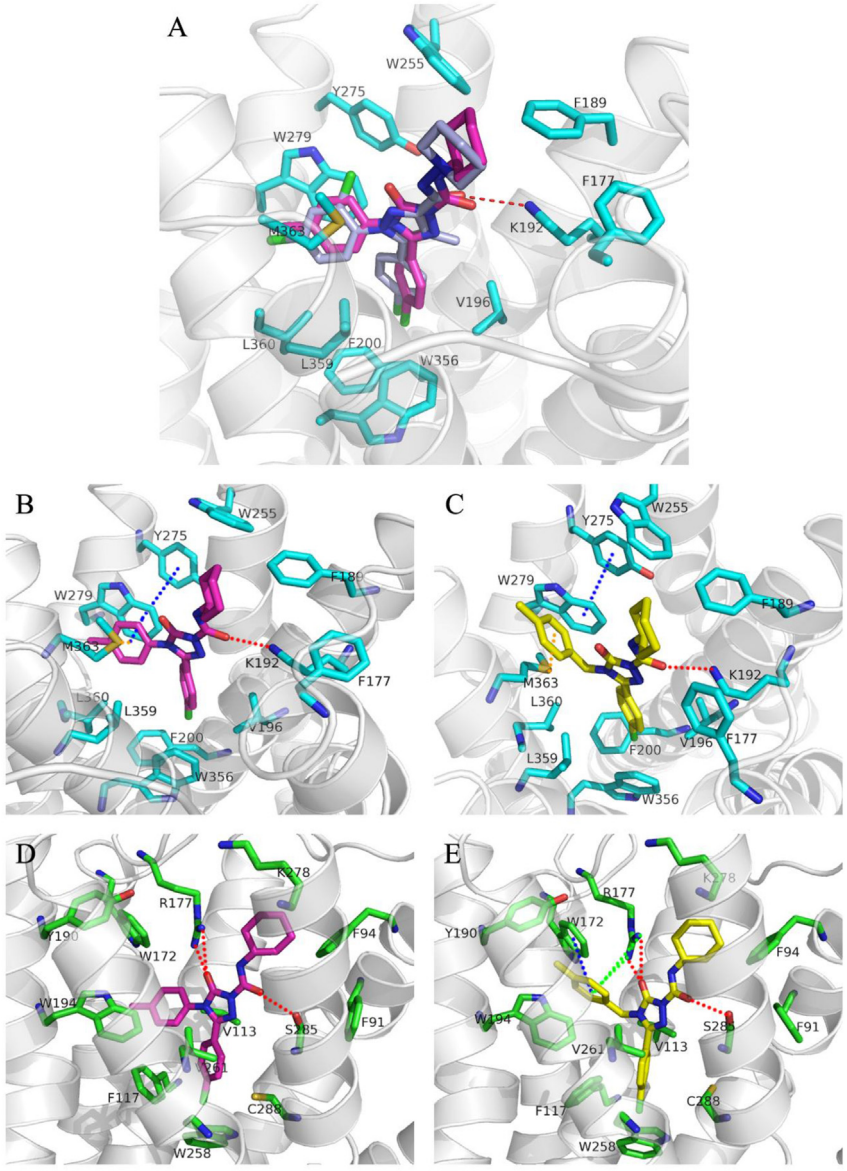

Fig. 8. (A) Superimposition of the docking results of CB1 receptor with SR141716A and **5c** based on backbone atoms, and docking results of CB1-**5c** (B), CB1-**5d** (C), CB2-**5c** (D), and CB2-**5d** (E) complexes. The carbon atoms of CB1 receptor, CB2 receptor, SR141716A, **5c**, and **5d** are colored by cyan, green, light blue, magentas, and yellow, respectively. The H-bonds are shown as red dashed lines, parallel π−π interactions are illustrated by blue dashed lines, cation-π interactions are displayed by green dashed lines, and S−π interactions are indicated by orange dashed lines. (For interpretation of the references to color in this figure legend, the reader is referred to the web version of this article.)

but only 46.4% CB2 receptor inhibition at 10 μM. While changing the building block to 4-methylbenzyl group, compound **5d** was a CB2 receptor selective antagonist with 3-fold lower bioactivity comparing with the reference compound JTE-907 under the same assay conditions, and it displayed only 42.6% CB1 receptor inhibitory effect at the concentration of 10 μM. Thus, comparative docking studies were carried out to better understand the binding modes between 1,2,4-triazolone derivatives and the CB receptors and to further predict possibly important residues affecting the selectivity.

As shown in Fig. 8B and C, K192 forms a hydrogen bond with the oxygen atom of amide group in both docking-simulated CB1-**5c** and CB1-**5d** complexes. For compound **5c**, the length and angle of the H-bond are 1.91 Å and 152.1°, respectively, and for **5d**, the values are 2.04 Å and 151.9°, correspondingly. The H-bond interaction implies the amide linker is necessary to maintain the activity for the CB1 receptor. The identical R_1 and R_3 subunits of both ligands display same interaction with CB1 receptor. Furthermore, it is observed distinctions between hydrophobic interactions producing by W279/M363 motif and the R_2 group with phenyl or benzyl group. In the CB1-**5c** complex, the *p*-tolyl group produces a face-to-face π–π interaction with W279, and in the meantime, W279 also forms π effect with the side chain of Y275. Whilst for ligand **5d**, the 4-methylbenzyl substituent interacts with W279 through a T-shaped π–π interaction, which is obviously weaker than parallel π–π interaction in the CB1-**5c** mode. In addition, a Met-aromatic interaction is formed between *p*-tolyl of **5c** and M363 with an S–π distance of 3.24 Å. However, in the CB1-**5d** complex, the S–π distance is 3.95 Å. Recently, Cordomí [62] reviewed the sulfur-containing amino acids which formed Met–Met and Met/Cys-aromatic interactions played a key role in pharmacology and function of seven-transmembrane receptors. In summary, changing R_2 unit may result in different interactions with residues W279 and M363, indicating these two residues could be important residues for the selectivity of ligand to the CB1 receptor.

Fig. 8D and E illustrate the docking simulation results of CB2-ligand complexes. The oxygen atom of amide forms H-bond with the hydroxyl group of S285, which is an important H-bond site for kinds of cannabinoid ligands [49,60]. For compounds **5c** and **5d**, the H-bond lengths and angles are 1.85 Å, 164.2° and 1.99 Å, 162.9°, respectively. In addition, the carboxyl group on the core ring can form another two H-bonds with R177 in the second extracellular loop (ECL2) with the bond lengths and angles of 2.41 Å, 137.0° and 1.95 Å, 153.3° in CB2-**5c** complex as well as 2.57 Å, 132.7° and 1.85 Å, 157.9° for CB2-**5d** interaction. Comparing to the binding mode of compound **5d** with the CB1 receptor, its R_3 cyclohexyl ring locates in a smaller hydrophobic pocket enclosed by F91, F94, and K278 of the CB2 receptor, which explains the relatively flexible cyclohexyl to be superior to the rigid phenyl group of other compound, like **5e** or **5i**, for the CB2 receptor bioactivity of ligand. In addition, the *p*-Cl phenyl group situates in the hydrophobic region encircled by V113, F117, W258, V261, and C288, which is similar with the CB1-ligand interaction mode. For the R_2 site, more apparent differentiations are obtained based on the docking simulations. For compound **5c**, the rigid R_2 structure leads to a handicap for proper contact with the pocket surrounded by the conserved aromatic residues W172, Y190, and W194, and no π–π interaction is observed from our modeling simulation results, which could be the major factor to induce the loss of its CB2 receptor bioactivity. By contrast, in docking simulated CB2-**5d** complex, the 4-methylbenzyl group deeply inserts into the corresponding pocket. A parallel π–π interaction forms between **5d**'s benzyl group and W172's indolyl ring with a distance of 4.42 Å. **5d**'s benzyl group also interacts with W194 via an edge-to-face π stacking. Meanwhile, R177 can form cation-π interaction to **5d**'s benzyl unit with a distance of 3.88 Å. The flexible docking studies indicated that the pocket formed by W172, R177, Y190, and W194 would be crucial to the ligand recognition of the CB2 receptor.

On the basis of the docking simulation results, the amide part is the significant H-bond forming site for both CB1 and CB2 receptors. For the 1,2,4-triazolone derivatives, the van der Waals interaction is the dominated binding mode with the conserved aromatic residues, including F3.36, W4.64, Y5.39, W5.43, and W6.48, of cannabinoid receptors. Comparing the docking-simulated interaction modes of compounds **5c** and **5d** binding to the CB1 or CB2 receptor, the selective property could be mainly caused by the interaction between R_2 group and the ambient residues, such as the residues W279 and M363 of the CB1 receptor and the residues W172, R177, and W194 of the CB2 receptor.

3. Conclusion

In the present work, a series of 1,2,4-triazolone derivatives was synthesized and evaluated for their *in vitro* cannabinoid receptor bioactivity. It was obtained of interesting antagonistic activity depending on various building blocks of the new compounds. Hence, we discovered that the 1,2,4-triazolone skeleton was a novel potential chemical scaffold for cannabinoid receptor antagonists. In order to gain a better understanding of the receptor-ligand interactions, homology models of both CB1 and CB2 receptors in active form were constructed based on the crystallized β2-adrenergic receptor, and the models were embedded in a DPPC/TIP3P bilayer system for the conformational refinements by MD simulations. The comparison of docking-calculated CB1-SR141716A and CB1-**5c** complexes implied the hydrophobic and aromatic interactions would be important for maintaining high CB1 receptor activity. Later, docking method was also applied to compute the binding modes between typical 1,2,4-triazolone ligands and each subtype of the CB receptors. The results indicated that K192 of the CB1 receptor and S285 of the CB2 receptor respectively formed H-bond with the oxygen atom of ligands' carboxyl group. Furthermore, W279 and M363 of the CB1 receptor as well as W172, R177, and W194 of the CB2 receptor displayed different interaction modes with the changed R_2 group, implying they might be important residues affecting the selectivity of ligand binding to cannabinoid receptors. By now, with the aim of identifying new drug candidate with better safety, the major task of developing cannabinoid ligands is improving selective property. The simulated binding modes of our synthesized compounds with the homology models of the CB1 and CB2 receptors in this work would be useful for understanding the interaction mechanism and designing new ligands with improved potency and selectivity.

4. Experimental section

4.1. Compound synthesis

4.1.1. Materials and instrumentation

Melting points were measured with a Büchi Melting Point B-540 apparatus (Büchi Labortechnik, Flawil, Switzerland) and are uncorrected. High-resolution LC-MS (HRMS) data were obtained using ESI ionization on Agilent 1290-6200 TOF LC-MS (Agilent, Palo Alto, CA, USA). Mass spectra (MS) were taken in ESI mode on Agilent 1100 LC-MS (Agilent, Palo Alto, CA, USA). ^{1}H NMR spectra was recorded on Bruker 500 MHz spectrometers (Bruker Bioscience, Billerica, MA, USA) using TMS as an internal standard. The values of chemical shifts (δ) were given in ppm and coupling constants (J) in Hz. The purity was determined by high-performance liquid chromatography (HPLC) performed on COSMOSIL C18-MS-II column (4.6 mm × 250 mm, 5 μm) using solvent of methanol/water at the

flow rate of 1 mL/min and peak detection at 254 nm under UV. All materials were used as received. Tetrahydrofuran (THF) and ether (Et_2O) were dried by distillation from sodium-benzophenone. Acetonitrile was dried by distillation from P_2O_5. All other solvents were used as received and were reagent grade where available.

*4.1.2. General procedure for synthesis of 4-substituted methyl benzoate derivatives **2a**–**2c***

4-substituted benzoic acid **1** (10 mmol) was refluxed in 10 mL MeOH catalyzed by sulfuric acid for 24 h. The solvent was concentrated *in vacuo*, and the crude product was purified by flash silica gel chromatography (petroleum ether/ethyl acetate = 10:1, v/v) to give the intermediates **2a**–**2c**.

*4.1.2.1. Methyl 4-chlorobenzoate (**2a**).* White solid. Yield: 87.3%. Melting Point: 38.6–39.9 °C (Ref. melting point 39 °C [63]).

*4.1.2.2. Methyl 4-methoxybenzoate (**2b**).* White solid. Yield: 93.6%. Melting Point: 46.4–48.5 °C (Ref. melting point 47–48 °C [64]).

*4.1.2.3. Methyl 4-methylbenzoate (**2c**).* White solid. Yield: 93.0%. Melting Point: 30.0–32.0 °C (Ref. melting point 32–35 °C [65]).

*4.1.3. General procedure for synthesis of 4-substituted benzohydrazide **3a**–**3c***

A solution of hydrazine hydrate (20.00 mmol) in 2 mL EtOH was added dropwise to the ester **2** (5.00 mmol). The mixture was refluxed for 5 h and filtered, and the corresponding acid hydrazide **3** was obtained by washing the residue with ice water.

*4.1.3.1. 4-Chlorobenzohydrazide (**3a**).* White solid. Yield: 93.4%. Melting Point: 162.0–163.7 °C (Ref. melting point 162–163 °C [66]).

*4.1.3.2. 4-Methoxybenzohydrazide (**3b**).* White solid. Yield: 70.0%. Melting Point: 138.0–139.7 °C (Ref. melting point 136–140 °C [67]).

*4.1.3.3. 4-Methylbenzohydrazide (**3c**).* White solid. Yield: 75.5%. Melting Point: 113.1–114.4 °C (Ref. melting point 112–114 °C [68]).

*4.1.4. General procedure for synthesis of 3,4-disubstituted 1h-1,2,4-triazol-5(4H)-one **4a**–**4g***

A stirred mixture of **3** (3.00 mmol) and 10 mL dry THF was warmed until a homogenous solution was obtained, and then isocyanate (3.60 mmol) was added via syringe. After being refluxed for 24 h, the mixture was diluted with Et_2O and the residue was collected by filtration. The precipitate was dissolved in 20 mL 1 N NaOH aqueous solution and refluxed for 24 h. The mixture was cooled in an ice bath and slowly acidified with 2 N HCl aqueous solution. The resulting precipitate was collected by filtration to give compound **4**.

*4.1.4.1. 3-(4-Chlorophenyl)-4-(4-methoxyphenyl)-1H-1,2,4-triazol-5(4H)-one (**4a**).* Brown solid. Yield: 53.5%. Melting Point: 204.2–205.8 °C. HRMS (ESI): *m/z* calcd for $C_{15}H_{12}ClN_3O_2$ $[M]^+$ 301.0618; found: *m/z* 301.0614. LCMS (ESI): $[M + H]^+$ 302.

*4.1.4.2. 3-(4-Chlorophenyl)-4-(p-tolyl)-1H-1,2,4-triazol-5(4H)-one (**4b**).* Light brown solid. Yield: 55.0%. Melting Point: 209.0–210.3 °C. LCMS (ESI): $[M + H]^+$ 286.

*4.1.4.3. 3-(4-Chlorophenyl)-4-(4-methylbenzyl)-1H-1,2,4-triazol-5(4H)-one (**4c**).* Offwhite solid. Yield: 64.1%. Melting point: >250 °C. LCMS (ESI): $[M + H]^+$ 300.

*4.1.4.4. 3-(4-Methoxyphenyl)-4-(p-tolyl)-1H-1,2,4-triazol-5(4H)-one (**4d**).* Light yellow solid. Yield: 54.5%. Melting Point: > 250 °C. LCMS (ESI): $[M + H]^+$ 282.

*4.1.4.5. 4-(4-Chlorophenyl)-3-(4-methoxyphenyl)-1H-1,2,4-triazol-5(4H)-one (**4e**).* Light yellow solid. Yield: 57.2%. Melting Point: 203.3–204.8 °C. LCMS (ESI): $[M + H]^+$ 302.

*4.1.4.6. 4-(4-Methylbenzyl)-3-(p-tolyl)-1H-1,2,4-triazol-5(4H)-one (**4f**).* Offwhite solid. Yield: 60.8%. Melting Point: > 250 °C. LCMS (ESI): $[M + H]^+$ 280.

*4.1.4.7. 4-(4-Chlorophenyl)-3-(p-tolyl)-1H-1,2,4-triazol-5(4H)-one (**4g**).* Light yellow solid. Yield: 82.4%. Melting Point: 207.9–208.9 °C. LCMS (ESI): $[M + H]^+$ 286.

*4.1.5. General procedure for synthesis of 1,2,4-triazolone derivatives **5a**–**m***

To a stirred solution of **4** (0.30 mmol) and 1,8-diazabicyclo[5.4.0] undec-7-ene (DBU) (0.60 mmol) in 3 mL dry acetonitrile under nitrogen was added dropwise isocyanate (0.36 mmol). After being refluxed overnight, the reaction was diluted with ethyl acetate. The reaction was transferred to a separatory funnel where it was washed three times with water and once with saturated aqueous sodium chloride solution. The organic layer was dried over anhydrous $MgSO_4$ before it was evaporated at reduced pressure. The resulting solid was purified by flash chromatography (petroleum ether/ethyl acetate = 3:1, v/v) to give the target compound **5a**–**m**.

*4.1.5.1. 3-(4-Chlorophenyl)-N-cyclohexyl-4-(4-methoxyphenyl)-5-oxo-4,5-dihydro-1H-1,2,4-triazole-1-carboxamide (**5a**).* Light yellow solid. Yield: 18.3%. Melting Point: 71.6–72.9 °C. HPLC (90% methanol in water): t_R = 5.986 min, 97.0%. ^1H NMR ($CDCl_3$, 500 MHz): δ 8.16 (d, J = 8.0 Hz, 1H), 7.38 (d, J = 8.0 Hz, 2H), 7.28 (d, J = 8.0 Hz, 2H), 7.15 (d, J = 8.5 Hz, 2H), 6.97 (d, J = 8.5 Hz, 2H), 3.95–3.89 (m, 1H), 3.85 (s, 3H), 2.00–1.98 (m, 2H), 1.73–1.70 (m, 2H), 1.60–1.58 (m, 1H), 1.44–1.31 (m, 4H), 1.27–1.26 (m, 1H). HRMS (ESI): *m/z* calcd for $C_{22}H_{23}ClN_4O_3$ $[M]^+$ 426.1459; found: *m/z* 426.1463.

*4.1.5.2. 3-(4-Chlorophenyl)-4-(4-methoxyphenyl)-5-oxo-N-(p-tolyl)-4,5-dihydro-1H-1,2,4-triazole-1-carboxamide (**5b**).* Light yellow solid. Yield: 15.6%. Melting point: 162.4–164.8 °C. HPLC (90% methanol in water): t_R = 5.379 min, 100.0%. ^1H NMR ($CDCl_3$, 500 MHz): δ 10.17 (s, 1H), 7.49 (d, J = 8.5 Hz, 2H), 7.38 (d, J = 8.5 Hz, 2H), 7.28 (d, J = 8.5 Hz, 4H), 7.24 (d, J = 8.5 Hz, 2H), 7.17 (d, J = 9.0 Hz, 4H), 6.99 (d, J = 9.0 Hz, 2H), 3.85 (s, 3H), 2.33 (s, 3H). HRMS (ESI): *m/z* calcd for $C_{23}H_{19}ClN_4O_3$ $[M]^+$ 434.1146; found: *m/z* 434.1151.

*4.1.5.3. 3-(4-Chlorophenyl)-N-cyclohexyl-5-oxo-4-(p-tolyl)-4,5-dihydro-1H-1,2,4-triazole-1-carboxamide (**5c**).* White solid. Yield: 19.1%. Melting point: 163.7–164.9 °C. HPLC (90% methanol in water): t_R = 5.892 min, 97.1%. ^1H NMR ($CDCl_3$, 500 MHz): δ 8.17 (d, J = 7.5 Hz, 1H), 7.35 (d, J = 8.5 Hz, 2H), 7.27 (d, J = 7.0 Hz, 4H), 7.10 (d, J = 7.5 Hz, 2H), 3.92–3.91 (m, 1H), 2.41 (s, 3H), 2.00–1.98 (m, 2H), 1.73–1.70 (m, 2H), 1.60–1.58 (m, 1H), 1.43–1.33 (m, 4H), 1.26–1.24 (m, 1H). HRMS (ESI): *m/z* calcd for $C_{22}H_{23}ClN_4O_2$ $[M]^+$ 410.1510; found: *m/z* 410.1512.

*4.1.5.4. 3-(4-Chlorophenyl)-N-cyclohexyl-4-(4-methylbenzyl)-5-oxo-4,5-dihydro-1H-1,2,4-triazole-1-carboxamide (**5d**).* White solid. Yield: 19.7%. Melting Point: 156.2–157.5 °C. HPLC (90% methanol in water): t_R = 7.922 min, 99.3%. ^1H NMR ($CDCl_3$, 500 MHz): δ 8.08 (d, J = 7.5 Hz, 1H), 7.44 (d, J = 8.5 Hz, 2H), 7.39 (d, J = 8.5 Hz, 2H), 7.12 (d, J = 8.0 Hz, 2H), 6.99 (d, J = 7.5 Hz, 2H), 4.88 (s, 2H), 3.89–3.87 (m,

1H), 2.32 (s, 3H), 2.03–2.00 (m, 2H), 1.74–1.71 (m, 2H), 1.61–1.59 (m, 1H), 1.44–1.30 (m, 4H), 1.26–1.22 (m, 1H). HRMS (ESI): *m/z* calcd for $C_{23}H_{25}ClN_4O_2$ $[M]^+$ 424.1666; found: *m/z* 424.1663.

*4.1.5.5. 3-(4-Chlorophenyl)-4-(4-methylbenzyl)-5-oxo-N-(p-tolyl)-4,5-dihydro-1H-1,2,4-triazole-1-carboxamide (**5e**).* Light yellow solid. Yield: 19.3%. Melting Point: 146.1–148.4 °C. HPLC (90% methanol in water): t_R = 7.235 min, 98.8%. ^{1}H NMR ($CDCl_3$, 500 MHz): δ 10.14 (s, 1H), 7.49 (dd, J = 7.5 Hz and 6.0 Hz, 4H), 7.41 (d, J = 8.0 Hz, 2H), 7.16 (t, J = 9.0 Hz, 4H), 7.03 (d, J = 7.5 Hz, 2H), 4.93 (s, 2H), 2.34 (s, 6H). HRMS (ESI): *m/z* calcd for $C_{24}H_{21}ClN_4O_2$ $[M]^+$ 432.1353; found: *m/z* 432.1358.

*4.1.5.6. N-Cyclohexyl-3-(4-methoxyphenyl)-5-oxo-4-(p-tolyl)-4,5-dihydro-1H-1,2,4-triazole-1-carboxamide (**5f**).* White solid. Yield: 38.0%. Melting Point: 193.6–194.7 °C. HPLC (90% methanol in water): t_R = 5.194 min, 95.8%. ^{1}H NMR ($CDCl_3$, 500 MHz): δ 8.18 (d, J = 7.5 Hz, 1H), 7.34 (d, J = 9.0 Hz, 2H), 7.24 (d, J = 8.0 Hz, 2H), 7.09 (d, J = 8.0 Hz, 2H), 6.77 (d, J = 9.0 Hz, 2H), 3.93–3.88 (m, 1H), 3.77 (s, 3H), 2.39 (s, 3H), 1.98–1.94 (m, 2H), 1.71–1.68 (m, 2H), 1.58–1.56 (m, 1H), 1.42–1.29 (m, 4H), 1.27–1.22 (m, 1H). HRMS (ESI): *m/z* calcd for $C_{23}H_{26}N_4O_3$ $[M]^+$ 406.2005; found: *m/z* 406.2011.

*4.1.5.7. N-(4-Chlorophenyl)-3-(4-methoxyphenyl)-5-oxo-4-(p-tolyl)-4,5-dihydro-1H-1,2,4-triazole-1-carboxamide (**5g**).* White solid. Yield: 13.9%. Melting Point: 91.0–92.6 °C. HPLC (90% methanol in water): t_R = 5.475 min, 100.0%. ^{1}H NMR ($CDCl_3$, 500 MHz): δ 10.34 (s, 1H), 7.35 (d, J = 9.0 Hz, 2H), 7.26 (d, J = 9.0 Hz, 4H), 7.11 (d, J = 8.0 Hz, 2H), 7.02 (d, J = 8.5 Hz, 2H), 6.89 (d, J = 8.0 Hz, 2H), 3.79 (s, 3H), 2.38 (s, 3H). HRMS (ESI): *m/z* calcd for $C_{23}H_{19}ClN_4O_3$ $[M]^+$ 434.1146; found: *m/z* 434.1150.

*4.1.5.8. N-Cyclohexyl-4-(4-methylbenzyl)-5-oxo-3-(p-tolyl)-4,5-dihydro-1H-1,2,4-triazole-1-carboxamide (**5h**).* Yellow solid. Yield: 27.5%. Melting Point: 99.3–100.8 °C. HPLC (90% methanol in water): t_R = 7.723 min, 97.4%. ^{1}H NMR ($CDCl_3$, 500 MHz): δ 8.10 (d, J = 8.0 Hz, 1H), 7.39 (d, J = 8.0 Hz, 2H), 7.21 (d, J = 8.0 Hz, 2H), 7.11 (d, J = 8.0 Hz, 2H), 7.00 (d, J = 8.0 Hz, 2H), 4.87 (s, 2H), 3.91–3.84 (m, 1H), 2.38 (s, 3H), 2.31 (s, 3H), 2.01–1.98 (m, 2H), 1.74–1.71 (m, 2H), 1.61–1.57 (m, 1H), 1.42–1.31 (m, 4H), 1.26–1.23 (m, 1H). HRMS (ESI): *m/z* calcd for $C_{24}H_{28}N_4O_2$ $[M]^+$ 404.2212; found: *m/z* 404.2215.

*4.1.5.9. N-(4-Chlorophenyl)-4-(4-methylbenzyl)-5-oxo-3-(p-tolyl)-4,5-dihydro-1H-1,2,4-triazole-1-carboxamide (**5i**).* Light yellow solid. Yield: 13.5%. Melting Point: 77.9–79.2 °C. HPLC (90% methanol in water): t_R = 7.416 min, 97.9%. ^{1}H NMR ($CDCl_3$, 500 MHz): δ 10.25 (s, 1H), 7.38 (d, J = 7.5 Hz, 2H), 7.28 (d, J = 9.0 Hz, 2H), 7.20 (d, J = 8.0 Hz, 2H), 7.12 (d, J = 8.0 Hz, 2H), 7.10 (d, J = 8.5 Hz, 2H), 6.99 (d, J = 8.0 Hz, 2H), 4.86 (s, 2H), 2.36 (s, 3H), 2.29 (s, 3H). HRMS (ESI): *m/z* calcd for $C_{24}H_{21}ClN_4O_2$ $[M]^+$ 432.1353; found: *m/z* 432.1356.

*4.1.5.10. 4-(4-Chlorophenyl)-N-cyclohexyl-5-oxo-3-(p-tolyl)-4,5-dihydro-1H-1,2,4-triazole-1-carboxamide (**5j**).* White solid. Yield: 37.1%. Melting Point: 161.0–162.3 °C. HPLC (90% methanol in water): t_R = 5.835 min, 100.0%. ^{1}H NMR ($CDCl_3$, 500 MHz): δ 8.09 (d, J = 7.5 Hz, 1H), 7.35 (d, J = 8.0 Hz, 2H), 7.28 (d, J = 8.0 Hz, 2H), 7.19 (d, J = 7.5 Hz, 2H), 7.02 (d, J = 8.0 Hz, 2H), 3.85–3.83 (m, 1H), 2.34 (s, 3H), 1.93–1.91 (m, 2H), 1.66–1.63 (m, 2H), 1.53–1.50 (m, 1H), 1.36–1.25 (m, 4H), 1.18–1.16 (m, 1H). HRMS (ESI): *m/z* calcd for $C_{22}H_{23}ClN_4O_2$ $[M]^+$ 410.1510; found: *m/z* 410.1512.

*4.1.5.11. 4-(4-Chlorophenyl)-5-oxo-N,3-di-p-tolyl-4,5-dihydro-1H-1,2,4-triazole-1-carboxamide (**5k**).* Yellow solid. Yield: 21.9%. Melting Point: 215.7–217.1 °C. HPLC (90% methanol in water): t_R = 6.812 min, 99.3%. ^{1}H NMR ($CDCl_3$, 500 MHz): δ 10.06 (s, 1H), 7.41 (dd, J = 8.5 Hz and 5.0 Hz, 4H), 7.33 (d, J = 9.5 Hz, 2H), 7.07 (dd, J = 8.5 Hz and 5.5 Hz, 4H), 6.95 (d, J = 8.5 Hz, 2H), 2.33 (s, 3H), 2.30 (s, 3H). HRMS (ESI): *m/z* calcd for $C_{23}H_{19}ClN_4O_2$ $[M]^+$ 418.1197; found: *m/z* 418.1195.

*4.1.5.12. 4-(4-Chlorophenyl)-3-(4-methoxyphenyl)-5-oxo-N-(p-tolyl)-4,5-dihydro-1H-1,2,4-triazole-1-carboxamide (**5l**).* Yellow solid. Yield: 38.6%. Melting Point: 144.8–145.6 °C. HPLC (90% methanol in water): t_R = 5.406 min, 97.9%. ^{1}H NMR ($CDCl_3$, 500 MHz): δ 10.09 (s, 1H), 7.49 (d, J = 8.5 Hz, 2H), 7.46 (d, J = 9.0 Hz, 2H), 7.35 (d, J = 8.5 Hz, 2H), 7.21 (d, J = 8.5 Hz, 2H), 7.17 (d, J = 8.0 Hz, 2H), 6.83 (d, J = 9.0 Hz, 2H), 3.81 (s, 3H), 2.33 (s, 3H). HRMS (ESI): *m/z* calcd for $C_{23}H_{19}ClN_4O_3$ $[M]^+$ 434.1146; found: *m/z* 434.1149.

*4.1.5.13. 4-(4-Chlorophenyl)-N-cyclohexyl-3-(4-methoxyphenyl)-5-oxo-4,5-dihydro-1H-1,2,4-triazole-1-carboxamide (**5m**).* Yellow solid. Yield: 13.9%. Melting Point: 98.4–99.5 °C. HPLC (90% methanol in water): t_R = 5.384 min, 100.0%. ^{1}H NMR ($CDCl_3$, 500 MHz): δ 8.07 (d, J = 8.0 Hz, 1H), 7.43 (d, J = 9.0 Hz, 2H), 7.32 (d, J = 9.0 Hz, 2H), 7.17 (d, J = 9.0 Hz, 2H), 6.81 (d, J = 9.0 Hz, 2H), 3.93–3.91 (m, 1H), 3.80 (s, 3H), 2.01–1.98 (m, 2H), 1.73–1.70 (m, 2H), 1.60–1.58 (m, 1H), 1.43–1.33 (m, 4H), 1.27–1.24 (m, 1H). HRMS (ESI): *m/z* calcd for $C_{22}H_{23}ClN_4O_3$ $[M]^+$ 426.1459; found: *m/z* 426.1462.

4.2. Biological assay

Chinese hamster ovarian (CHO) cells stably co-expressing Gα15/16 with either CB1 or CB2 receptor were plated onto 96-well plates and incubated for 24 h. Cells were loaded with 2 μM fluo-4 AM in Hanks balanced salt solution (HBSS, containing 5.4 mM KCl, 0.3 mM Na_2HPO_4, 0.4 mM KH_2PO_4, 4.2 mM $NaHCO_3$, 1.3 mM $CaCl_2$, 0.5 mM $MgCl_2$, 0.6 mM $MgSO_4$, 137 mM NaCl, 5.6 mM D-glucose and 250 μM sulfinpyrazone, pH 7.4) at 37 °C for 45 min. After moving the excess dye, cells were washed with HBSS and 50 μL HBSS containing variable concentrations of test compounds (10 pM–100 μM), Rimonabant, JTE-907 (positive control) or DMSO (negative control) was added. After 10 min incubation at room temperature, 25 μL CP55940 was dispensed into the wells using a FlexStation microplate reader, and intracellular calcium change was recorded at an excitation wavelength of 485 nm and an emission wavelength of 525 nm. All experiments were performed in triplicate. IC_{50} values were analyzed with sigmoidal dose–response curve fitting using GraphPad Prism.

4.3. Computational methods

4.3.1. Homology models of both CB1 and CB2 receptors

The sequences of CB1 and CB2 receptors were got from the NCBI protein database. Owing to the flexibility of the N- and C-terminal domains as well as no direct receptor-ligand interaction reported for these regions, residues 109–417 of CB1 receptor and residues 26–319 of CB2 receptor were used for the setup of the homology models. The X-ray structure of human β2-adrenergic receptor (PDB code: 2RH1, resolution = 2.40 Å) was downloaded from the RCSB Protein Data Bank website (http://www.pdb.org) as the basic template. Considering both CB1 and CB2 receptors contain many of the structurally conserved motifs associated with GPCRs, as shown in Fig. 4, the sequential alignment was carried out based on the structural characterization of 2RH1. Since the seven transmembrane helical regions of GPCRs are highly conserved, the coordinates for the residues in these regions of β2-AR were directly assigned to the corresponding residues of CB receptors using DS 2.5.5/protein module [56]. The conformations of extracellular and

intracellular loops were obtained through the loop search method, and the beginning and ending regions were generated by endpair module.

4.3.2. MD Simulations

Each of the initial homology models was inserted into a pre-equilibrated DPPC/TIP3P hydrate bilayer membrane system by CHARMM GUI Membrane Builder (http://www.charmm-gui.org/) [54,69]. The refinement and minimization of CB receptor homology models was performed by molecular dynamics using Amber 11 package [53]. The force field parameters for DPPC molecule were created using general Amber force field (GAFF) [70] and restrained electrostatic potential (RESP) partial charges [71], and the AMBER ff99SB force field [72] was selected for the proteins. Chloride ions were added to the system until neutrality was achieved.

Each system was minimized in two steps. First, the whole protein was kept fixed with a force constant of 300 kcal/(mol Å), while the lipids, water, and ions were allowed to minimize, and second, only the atoms of backbone were restrained with a force of 50 kcal/(mol Å). In each step, the minimization was perform by the steepest descent algorithm for 1000 steps and then conjugated gradient method for another 5000 steps. Later, the systems were gradually heated from 0 to 300 K over 100 ps in the NVT ensemble. Then, equilibration of each system was performed in an NPT ensemble at 300 K under 1.0 atm pressure. During this procedure, the force restraint weight to the atoms of backbone was decreased from 50 to 1 kcal/(mol Å) gradually over total 3500 ps.

Finally, 30 ns production MD simulations were carried out for the protein/DPPC/TIP3P systems in the NPT ensemble at a temperature of 300 K and a pressure of 1 atm. Considering our homology models are apo proteins in the active state, in the production process the atoms of backbone in the 7-TM regions were still restrained with a force constant of 1 kcal/(mol Å) to maintain the active conformation. All the MD simulations were performed with the integration time step of 2 fs, and the coordinates and velocities were saved every 2 ps.

4.3.3. Flexible docking calculations

The aforementioned MD refined CB receptor homology models were employed for molecular docking studies. The active pockets of the receptors were predicted based on the combination of Connolly solvent-accessible protein channel analysis in the Sybyl-X1.3/MOLCAD program [57] and the literature data [43,60]. The initial structures of **5c** and **5d** were constructed by SKETCH module of Sybyl-X1.3 [57], and minimized by Tripos force field with Gasteiger-Hückel atomic charge. Then the ligands were put into the binding cavities surrounded by the helices III, V, VI, and VII of the two receptors, respectively. All the single bonds of the ligand as well as the side chains of residues inside the binding pocket were regarded as rotatable bonds, and the H-bonding sites were marked for suitable atoms of both receptor and ligand. Flexible docking of each compound with either CB1 or CB2 receptor was performed applying Sybyl-X1.3/FlexiDock [57] program to search the possible binding conformations of ligands and receptors. The binding interaction energy was calculated including the terms of van der Waals, electrostatics, and torsion energy defined in the Tripos force field, and top 20 scored receptor-ligand complexes were kept for further analysis.

Acknowledgments

We wish to thank the National Natural Science Foundation of China (No. NSFC 30973637) and Qianjiang talents project of technology office in Zhejiang province (No. 2010R10048) for funding our work.

Appendix A. Supplementary data

Supplementary data related to this article can be found at http://dx.doi.org/10.1016/j.ejmech.2013.12.018.

References

[1] P.H. Reggio, Curr. Med. Chem. 17 (2010) 1468–1486.
[2] R.G. Pertwee, Pharmacol. Ther. 74 (1997) 129–180.
[3] G.A. Thakur, R. Tichkule, S. Bajaj, A. Makriyannis, Expert Opin. Ther. Pat. 19 (2009) 1647–1673.
[4] M. Maccarrone, G. Bernardi, A.F. Agrò, D. Centonze, Brit. J. Pharmacol. 163 (2011) 1379–1390.
[5] R. Tanasescu, C.S. Constantinescu, Immunobiology 215 (2010) 588–597.
[6] P. Caraceni, M. Domenicali, F. Giannone, M. Bernardi, Best Pract. Res. Cl. En. 23 (2009) 65–77.
[7] P. Anand, G. Whiteside, C.J. Fowler, A.G. Hohmann, Brain Res. Rev. 60 (2009) 255–266.
[8] M. Odan, N. Ishizuka, Y. Hiramatsu, M. Inagaki, H. Hashizume, Y. Fujii, S. Mitsumori, Y. Morioka, M. Soga, M. Deguchi, K. Yasui, A. Arimura, Bioorg. Med. Chem. Lett. 22 (2012) 2803–2806.
[9] P. Yang, K.-Z. Myint, Q. Tong, R. Feng, H. Cao, A.A. Almehizia, M.H. Alqarni, L. Wang, P. Bartlow, Y. Gao, J. Gertsch, J. Teramachi, N. Kurihara, G.D. Roodman, T. Cheng, X.-Q. Xie, J. Med. Chem. 55 (2012) 9973–9987.
[10] Q. Ouyang, Q. Tong, R. Feng, K.-Z. Myint, P. Yang, X.-Q. Xie, ACS Med. Chem. Lett. 4 (2013) 387–392.
[11] P. Yang, L. Wang, R. Feng, A.A. Almehizia, Q. Tong, K.-Z. Myint, Q. Ouyang, M.H. Alqarni, L. Wang, X.-Q. Xie, J. Med. Chem. 56 (2013) 2045–2058.
[12] G. Kunos, J. Tam, Br. J. Pharmacol. 163 (2011) 1423–1431.
[13] M. Alvarado, J. Decara, M.J. Luque, L. Hernandez-Folgado, M. Gomez-Cañas, M. Gomez-Ruiz, J. Fernandez-Ruiz, J. Elguero, N. Jagerovic, A. Serrano, P. Goya, F.R. de Fonseca, Bioorg. Med. Chem. 21 (2013) 1708–1716.
[14] D. Jones, Nat. Rev. Drug. Discov. 7 (2008) 961–962.
[15] Y.-K. Wu, C.-F. Yeh, T.W. Ly, M.-S. Hung, Curr. Top. Med. Chem. 11 (2011) 1421–1429.
[16] P. Pacher, S. Batkai, G. Kunos, Pharmacol. Rev. 58 (2006) 389–462.
[17] M. Rinaldi-Carmona, F. Barth, M. Heaulme, D. Shire, B. Calandra, C. Congy, S. Martinez, J. Maruani, G. Neliat, FEBS Lett. 350 (1994) 240–244.
[18] M. Rinaldi-Carmona, F. Barth, J. Millan, J.-M. Derocq, P. Casellas, C. Congy, D. Oustric, M. Sarran, M. Bouaboula, B. Calandra, M. Portier, D. Shire, J.-C. Brelière, G. Le Fur, J. Pharmacol. Exp. Ther. 284 (1998) 644–650.
[19] M. Portier, M. Rinaldi-Carmona, F. Pecceu, T. Combes, C. Poinot-Chazel, B. Calandra, F. Barth, G. Le Fur, P. Casellas, J. Pharmacol. Exp. Ther. 288 (1999) 582–589.
[20] H.J. Seo, M.J. Kim, S.H. Lee, S.-H. Lee, M.E. Jung, M.-S. Kim, K. Ahn, J. Kim, J. Lee, Bioorg. Med. Chem. 18 (2010) 1149–1162.
[21] P.K. Sasmal, R. Talwar, J. Swetha, D. Balasubrahmanyam, B. Venkatesham, K.A. Rawoof, B. Neelima Devi, V.P. Jadhav, S.K. Khan, P. Mohan, D. Srinivasa Reddy, V.K. Nyavanandi, S. Nanduri, K. Shiva Kumar, M. Kannan, P. Srinivas, P. Nadipalli, H. Chaudhury, V.J. Sebastian, Bioorg. Med. Chem. Lett. 21 (2011) 4913–4918.
[22] F. Piscitelli, A. Ligresti, G. La Regina, V. Gatti, A. Brizzi, S. Pasquini, M. Allarà, M.A. Maria Carai, E. Novellino, G. Colombo, V. Di Marzo, F. Corelli, R. Silvestri, Eur. J. Med. Chem. 45 (2011) 5641–5653.
[23] S.R. Donohue, R.F. Dannals, C. Halldin, V.W. Pike, J. Med. Chem. 54 (2011) 2961–2970.
[24] A. Fulp, K. Bortoff, H. Seltzman, Y. Zhang, J. Mathews, R. Snyder, T. Fennell, R. Maitra, J. Med. Chem. 55 (2012) 2820–2834.
[25] J. Bostrom, K. Berggren, T. Elebring, P.J. Greasley, M. Wilstermann, Bioorg. Med. Chem. 15 (2007) 4077–4084.
[26] J.H.M. Lange, M.A.W. van der Neut, A.J.M. Borst, M. Yildirim, H.H. van Stuivenberg, B.J. van Vliet, C.G. Kruse, Bioorg. Med. Chem. Lett. 20 (2010) 2770–2775.
[27] R.A. Smith, Z. Fathi, S.-E. Brown, S. Choi, J. Fan, S. Jenkins, H.C.E. Kluender, A. Konkar, R. Lavoie, R. Mays, J. Natoli, S.J. O'Connor, A.A. Ortiz, B. Podlogar, C. Taing, S. Tomlinson, T. Tritto, Z. Zhang, Bioorg. Med. Chem. Lett. 17 (2007) 673–678.
[28] L. Botta, T. Semeraro, C. Mugnaini, A. Ligresti, E. Palazzo, S. Maione, V. Di Marzo, F. Corelli, J. Med. Chem. 51 (2008) 5075–5084.
[29] H. Omura, M. Kawai, A. Shima, Y. Iwata, F. Ito, T. Masuda, A. Ohta, N. Makita, K. Omoto, H. Sugimoto, A. Kikuchi, H. Iwata, K. Ando, Bioorg. Med. Chem. Lett. 18 (2008) 3310–3314.
[30] V. Gembus, C. Furman, R. Millet, R. Mansouri, P. Chavatte, V. Levacher, J.-F. Brière, Eur. J. Med. Chem. 58 (2012) 396–404.
[31] A.J. Morrison, J.M. Adam, J.A. Baker, R.A. Campbell, J.K. Clark, J.E. Cottney, M. Deehan, A.-M. Easson, R. Fields, S. Francis, F. Jeremiah, N. Keddie, T. Kiyoi, D.R. McArthur, K. Meyer, P.D. Ratcliffe, J. Schulz, G. Wishart, K. Yoshiizumi, Bioorg. Med. Chem. Lett. 21 (2011) 506–509.

[32] J.-Z. Chen, X.-W. Han, Q. Liu, A. Makriyannis, J. Wang, X.-Q. Xie, J. Med. Chem. 49 (2006) 625–636.
[33] V. Cherezov, D.M. Rosenbaum, M.A. Hanson, S.G.F. Rasmussen, F.S. Thian, T.S. Kobilka, H.-J. Choi, P. Kuhn, W.I. Weis, B.K. Kobilka, R.C. Stevens, Science 318 (2007) 1258–1265.
[34] M. Jansen, H. Rabe, A. Strehle, S. Dieler, F. Debus, G. Dannhardt, M.H. Akabas, H. Lüddens, J. Med. Chem. 51 (2008) 4430–4448.
[35] J.M. Kane, B.M. Baron, M.W. Dudley, S.M. Sorensen, M.A. Staeger, F.P. Miller, J. Med. Chem. 33 (1990) 2772–2777.
[36] J.M. Kane, Synthesis 10 (1987) 912–914.
[37] K.S. Schroeder, B.D. Neagle, J. Biomol. Screen. 1 (1996) 75–80.
[38] L.C. Mattheakis, L.D. Ohler, Drug. Discov. Today 5 (Suppl. 1) (2000) 15–19.
[39] G.R. Monteith, G.S.J. Bird, Trends Pharmacol. Sci. 26 (2005) 218–223.
[40] T. Zhu, L.-Y. Fang, X. Xie, Acta Pharmacol. Sin. 29 (2008) 507–516.
[41] H. Iwamura, H. Suzuki, Y. Ueda, T. Kaya, T. Inaba, J. Pharm. Pharm. Sci. 296 (2001) 420–425.
[42] X.-Q. Xie, J.-Z. Chen, E.M. Billings, Proteins 53 (2003) 307–319.
[43] O.M.H. Salo, M. Lahtela-Kakkonen, J. Gynther, T. Jaervinen, A. Poso, J. Med. Chem. 47 (2004) 3048–3057.
[44] T. Tuccinardi, P.L. Ferrarini, C. Manera, G. Ortore, G. Saccomanni, A. Martinelli, J. Med. Chem. 49 (2006) 984–994.
[45] C. Montero, N.E. Campillo, P. Goya, J.A. Páez, Eur. J. Med. Chem. 40 (2005) 75–83.
[46] P. Diaz, S.S. Phatak, J. Xu, F. Astruc-Diaz, C.N. Cavasotto, M. Naguib, J. Med. Chem. 52 (2009) 433–444.
[47] S. Durdagi, M. Papadopoulos, P. Zoumpoulakis, C. Koukoulitsa, T. Mavromoustakos, Mol. Divers. 14 (2010) 257–276.
[48] N.A. Osman, A.H. Mahmoud, M. Allar, R. Niess, K.A. Abouzid, V. Di Marzo, A.H. Abadi, Bioorg. Med. Chem. 18 (2010) 8463–8477.
[49] E. Cichero, A. Ligresti, M. Allar, V. di Marzo, Z. Lazzati, P. D'Ursi, A. Marabotti, L. Milanesi, A. Spallarossa, A. Ranise, P. Fossa, Eur. J. Med. Chem. 46 (2011) 4489–4505.
[50] G. Kuang, G. Hu, X. Sun, W. Li, G. Liu, Y. Tang, J. Mol. Model. 18 (2012) 3831–3845.
[51] K.-i. Kusakabe, Y. Tada, Y. Iso, M. Sakagami, Y. Morioka, N. Chomei, S. Shinonome, K. Kawamoto, H. Takenaka, K. Yasui, H. Hamana, K. Hanasaki, Bioorg. Med. Chem. 21 (2013) 2045–2055.
[52] D. Shire, B.C.M. Delpech, X. Dumont, M. Kaghad, G. Le Fur, D. Caput, P. Ferrara, J. Biol. Chem. 271 (1996) 6941–6946.
[53] D.A. Case, T.E. Cheatham, T. Darden, H. Gohlke, R. Luo, K.M. Merz, C. Simmerling, B. Wang, AMBER 11, University of California, San Francisco, 2010.
[54] S. Jo, T. Kim, W. Im, PLoS ONE 2 (2007) e880.
[55] R. Liithy, J.U. Bowie, D. Eisenberg, Nature 356 (1992) 83–85.
[56] 2.5.5, Accelrys Discovery Studio, Accelrys Software Inc., San Diego, CA, 2010.
[57] ver. x1.3, Sybyl Molecular Modeling Software Packages, Tripos Associates, Inc., St. Louis, MO63144, 2011.
[58] S.D. McAllister, G. Rizvi, S. Anavi-Goffer, D.P. Hurst, J. Barnett-Norris, D.L. Lynch, P.H. Reggio, M.E. Abood, J. Med. Chem. 46 (2003) 5139–5152.
[59] S.D. McAllister, Q. Tao, J. Barnett-Norris, K. Buehner, D.P. Hurst, F. Guarnieri, P.H. Reggio, K.W. Nowell Harmon, G.A. Cabral, M.E. Abood, Biochem. Pharmacol. 63 (2002) 2121–2136.
[60] O.M.H. Salo, K.H. Raitio, J.R. Savinainen, T. Nevalainen, M. Lahtela-Kakkonen, J.T. Laitinen, T. Jaervinen, A. Poso, J. Med. Chem. 48 (2005) 7166–7171.
[61] J.-J. Chen, S. Han, Y. Cao, J.-Z. Chen, Acta Pharm. Sin. 48 (2013) 1436–1449.
[62] A. Cordomí, J.C. Gómez-Tamayo, V. Gigoux, D. Fourmy, Trends Pharmacol. Sci. 34 (2013) 320–331.
[63] G.A. Olah, S.C. Narang, A. Garcia-Luna, Synthesis 1981 (1981) 790–791.
[64] N. Maraš, S. Polanc, M. Kočevar, Tetrahedron 64 (2008) 11618–11624.
[65] W.J. Bailey, R. Barclay, J. Am. Chem. Soc. 81 (1959) 5393–5396.
[66] J.P. Horwitz, V.A. Grakauskas, J. Org. Chem. 19 (1954) 194–201.
[67] F. Macaev, G. Rusu, S. Pogrebnoi, A. Gudima, E. Stingaci, L. Vlad, N. Shvets, F. Kandemirli, A. Dimoglo, R. Reynolds, Bioorg. Med. Chem. 13 (2005) 4842–4850.
[68] A. Omodei-Sale, P. Consonni, G. Galliani, J. Med. Chem. 26 (1983) 1187–1192.
[69] T.B. Woolf, B. Roux, Proteins 24 (1996) 92–114.
[70] J. Wang, R.M. Wolf, J.W. Caldwell, P.A. Kollman, D.A. Case, J. Comput. Chem. 25 (2004) 1157–1174.
[71] C.I. Bayly, P. Cieplak, W. Cornell, P.A. Kollman, J. Phys. Chem. 97 (1993) 10269–10280.
[72] V. Hornak, R. Abel, A. Okur, B. Strockbine, A. Roitberg, C. Simmerling, Proteins 65 (2006) 712–725.